Bias in Differential Reflectivity Revealed With a Numerical Model of a Polarimetric Phased Array Antenna

Djordje Mirkovic and Dusan S. Zrnic, *Life Fellow, IEEE*

***Abstract*— An electromagnetic simulation of a large polarimetric phased array radar antenna for weather observation using a full-wave electromagnetic solver is presented. The modeled antenna is part of a Ten Panel Demonstrator (TPD) radar serving as a proof of concept for the Advanced Technology Demonstrator (ATD). The simulations we use to compute copolar and cross-polar patterns at horizontal and vertical polarizations. We present these patterns for beam pointing broadside, in a horizontal principal plane, and out of the principal plane. Then we include these patterns into existing exact and approximate formulas to quantify bias in differential reflectivity and show the difference in bias for a few pointing directions of the antenna beam. We demonstrate the techniques which do not use a full-wave electromagnetic approach and are based on infinite array assumption to generate accurate copolar patterns but fail to replicate the cross-polar patterns. The latter ones are crucial for weather applications because they induce bias in polarimetric variable estimates. Finally, we compare the simulation times needed to model one antenna panel with other commonly used solvers.**

***Index Terms*— Polarimetric phased array radar, polarimetric variables, polarimetric bias, differential reflectivity bias.**

I. Introduction

THE most advanced technology for weather surveillance with radar is the Polarimetric Phased Array Radar (PPAR). NOAA has been exploring this option for almost two decades [1], [2], [3], [4]. Its advantages are speed of volume coverage, adaptation to scan when and where needed, including designs of transmit waveforms, and received signal processing matched to the phenomena of interest. Its biggest challenge is achieving polarimetric measurements with quality matching the WSR-88Ds'. This is especially hard for a PPAR with a planar array antenna due to the dependence of polarization on the antenna pointing direction [5], [6], [7]. A further complication is the preferred polarimetric mode for weather observations. That mode is the simultaneous transmission and reception of the horizontal (H) and vertical (V) (SHV) polarized fields. The isolation requirement between the polarization signals is about twice as large in the SHV mode compared to the mode where the polarization on transmission is alternating (AHV mode).

Nonetheless, the errors of the radar variables for a substantial range of operating conditions are significantly larger in the AHV mode [8]. Therefore, the SHV is the preferred choice for research and future operational PPARs. Our study examines the antenna patterns from NOAA's PPAR dubbed Ten Panel Demonstrator (TPD). The TPD was meant to serve as proof of concept to build a more substantial PPAR called the Advanced Technology Demonstrator (ATD), [9].

The important causes of biases in polarimetric variables obtained with planar PPARs are as follows. 1) Mismatch in the copolar main lobes (shape and pointing direction) of the antenna patterns [10], [11], [12]. 2) Geometrically induced bias due to nonorthogonality of transmitted fields [8]. 3) Geometrically induced bias due to deviation of the intended horizontally/vertically polarized fields from the true horizontal /vertical direction [4]. 4) Cross-polar patterns [13]. 5) System hardware. The number 2 and 3 effects combine, and acceptable corrections can be made if the lobes' peak positions and values of the intended H and V patterns are known.

Theoretical expressions for bias in differential reflectivity [13] and copolar correlation coefficient [14] induced by cross-polar patterns are available, but no experimental verification has been made on PPARs. Measuring cross-polar patterns on large arrays in the far field is demanding as the signals may be weak and easily contaminated by interferences. Although near-field measurements are easier to make, they also may have limitations in quantifying cross-polar patterns related to the correction of the probe's cross-polar pattern [15], [16] they are time-consuming and unsuitable for antennas in the field.

An alternate way for obtaining the radiation patterns is via electromagnetic (EM) simulation. These can complement measurements and have the following advantages. Ease and speed in quantifying changes in patterns of antennas with failed elements and guiding antenna designers by isolating

Manuscript received 1 February 2023; revised 2 June 2023; accepted 24 July 2023. Date of publication 15 August 2023; date of current version 14 September 2023. This work was supported by the NOAA/Office of Oceanic and Atmospheric Research through the NOAA-University of Oklahoma, U.S. Department of Commerce, under Grant NA21OAR4320204. *(Corresponding author: Djordje Mirkovic.)*

Djordje Mirkovic is with the Cooperative Institute for Severe and High-Impact Weather Research and Operations, The University of Oklahoma, Norman, OK 73072 USA, and also with the NOAA/OAR National Severe Storms Laboratory, Norman, OK 73072 USA (e-mail: Djordje.Mirkovic@noaa.gov).

Dusan S. Zrnic is with the NOAA/OAR National Severe Storms Laboratory, Norman, OK 73072 USA, and also with the School of Meteorology and the School of Electrical and Computer Engineering, The University of Oklahoma, Norman, OK 73072 USA (e-mail: Dusan.Zrnic@noaa.gov).

Digital Object Identifier 10.1109/TRS.2023.3305490

issues, incorporating changes, checking effects on pattern performance, and assessing bias in polarimetric variables before building the antenna.

EM simulations also have some limitations, including the assumption that all radiators are the same and there are no variations across the array due to manufacturing and/or other imperfections. The other limitation is the complexity of a detailed simulation of very large arrays. To mitigate the latter, engineers typically resort to approximate techniques combining simulations of the embedded element pattern with the array factor. Finally, it is unlikely that EM simulations could capture the effects of active components in the antenna backplane (e.g., T/R elements), which also affect antenna pattern measurements. Nonetheless, the fact that EM simulations typically capture the effects of passive antenna components (e.g., patch radiators and mutual couplings) can provide a unique insight into the antenna pattern properties that are devoid of the effects caused by the active electronic components.

Before considering the full TPD array antenna, we modeled the single element patterns, central embedded element patterns in an 8×8 panel with the rest of the panel load matched, and full panel patterns [6], [17]. The investigation in [17] showed a very good agreement between modeled and measured patterns of the single element and single panel. This increased confidence in our modeling approach and led us to model the full TPD antenna.

Here we demonstrate potency in simulating patterns of a large PPAR antenna (the TPD) with a commercially available WIPL-D 3D EM solver [18]. At pointing directions out of the principal planes, obtaining credible cross-polar patterns is impossible with approximate solutions. The important results from our model are the pattern's amplitudes and phases. These are crucial for assessing the antenna-induced biases in the polarimetric variables. Hence we use the simulated patterns to estimate this bias in the differential reflectivity and correlation coefficient between the H and V polarized returns from radars operating in the SHV mode. We quantify the effects of cross-polar patterns and beam pointing on the differential reflectivity and correlation coefficient bias.

The paper is organized as follows. The second section contains the effects of antenna patterns on bias in differential reflectivity and correlation coefficient. The radar antenna and its model are described in section three, where a short description of computational efficiency is included. In the fourth section, we consider some weather observations using TPD. Section five concludes the paper.

II. Effects of Antenna Patterns on the Polarimetric Variable Bias

Assume the SHV mode of polarimetric measurement. Unit excitation voltage of transmit element is $[\,1\ e^{j\beta}\,]^T$, (T signifies transpose), a phase difference β between the transmitted H and V components, and no coupling on reflection. Ignoring this coupling enables fair comparison of the system effects (i.e., separation of these from the environment). Also, assume that transmit and receive patterns for each polarization are identical. Then the incremental received voltages from scatterers in incremental parts of radar resolution volume are (as in [13]).

$$\begin{bmatrix} \delta V_{\rm h}(t,r) \\ \delta V_{\rm v}(t,r) \end{bmatrix} = \overrightarrow{V} = \boldsymbol{F}^T \boldsymbol{S} \boldsymbol{F} \overrightarrow{E} = \begin{bmatrix} F_{\rm hh} & F_{\rm vh} \\ F_{\rm hv} & F_{\rm vv} \end{bmatrix} \begin{bmatrix} s_{\rm hh} e^{-{\rm j}\Phi_{\rm DP}} & 0 \\ 0 & s_{\rm vv} \end{bmatrix} \begin{bmatrix} F_{\rm hh} & F_{\rm hv} \\ F_{\rm vh} & F_{\rm vv} \end{bmatrix} \begin{bmatrix} 1 \\ e^{{\rm j}\beta} \end{bmatrix}, \tag{1}$$

where the backscattering matrix coefficient $s_{hh} = \sum_i s_{hh}^{(i)} e^{-j2kr_i}$ is the sum of coefficients from individual scatterers, r_i is the range to the scatterer, and the wave number $k = 2\pi/\lambda$. The subscript on the left side of (1) stands for polarization. The second subscript on the scattering coefficients $s_{\rm ij}$ and radiation patterns $F_{\rm ij}$ indicates the intended (incident) polarization, and the first stands for the achieved (scattered) polarization. Further, the gain is related to the pattern via

$$G_{\rm ij}(\theta,\phi) = \frac{4\pi}{Z_0}\eta \left| F_{\rm ij}(\theta,\phi) \right|^2. \tag{2}$$

The angle pair θ, ϕ is in accord with standard notation (θ with respect to the vertical $z-$axis, ϕ with respect to the horizontal axis x) Z_0 is the free-space impedance, and η is the antenna efficiency factor.

$$\begin{aligned} \frac{P_{\rm h}}{\langle |s_{\rm vv}|^2 \rangle} = Z_{\rm dr} \int_\Omega \Big\{ & |F_{\rm hh}|^2 \big[|F_{\rm hh}|^2 + 2Re\big(F_{\rm hh}^* F_{\rm hv} e^{j\beta}\big) + |F_{\rm hv}|^2 \big] \\ & + 2\rho_{\rm hv} Z_{\rm dr}^{-\frac{1}{2}} Re\Big[e^{j\Phi_{\rm DP}} \Big(F_{\rm hh}^2 F_{\rm vh}^{*\,2} + F_{\rm hh} F_{\rm hv} F_{\rm vh}^{*\,2} e^{j\beta} \\ & + F_{\rm hh}^2 F_{\rm vh}^* F_{\rm vv}^* e^{-j\beta} + F_{\rm hh} F_{\rm hv} F_{\rm vh}^* F_{\rm vv}^* \Big) \Big] \\ & + Z_{dr}^{-1} \big[|F_{\rm vh}|^2 \big[|F_{\rm vh}|^2 + 2Re\big(F_{\rm hv} F_{\rm vv}^* e^{-j\beta}\big) + |F_{\rm vv}|^2 \big] \big] \Big\} \\ & \times d\Omega, \end{aligned} \tag{3a}$$

$$\begin{aligned} \frac{P_{\rm v}}{\langle |s_{\rm vv}|^2 \rangle} = \int_\Omega \Big\{ & Z_{\rm dr} |F_{\rm hv}|^2 \big[|F_{\rm hh}|^2 + 2Re\big(F_{\rm hh} F_{\rm hv}^* e^{-j\beta}\big) + |F_{\rm hv}|^2 \big] \\ & + 2\rho_{\rm hv} Z_{\rm dr}^{\frac{1}{2}} Re\Big\{ e^{j\Phi_{\rm DP}} \big[F_{\rm hh} F_{\rm hv} F_{\rm vv}^* F_{\rm vh}^* + F_{\rm hv}^2 F_{\rm vv}^* F_{\rm vh}^* e^{j\beta} \\ & + F_{\rm hh} F_{\rm hv} F_{\rm vv}^{*\,2} e^{-j\beta} + F_{\rm hv}^2 F_{\rm vv}^{*\,2} \big] \Big\} \\ & + |F_{\rm vv}|^2 \big[|F_{\rm vh}|^2 + 2Re\big\{ F_{\rm vh} F_{\rm vv}^* e^{-j\beta} \big\} + |F_{\rm vv}|^2 \big] \Big\} d\Omega, \end{aligned} \tag{3b}$$

From (1), we can derive the received powers at each polarization similar to [13] but with some differences. The authors in [13], consider a special case where $F_{\rm hh}$ and $F_{\rm vv}$ are real, within the main lobe, and the cross-polar components $F_{\rm hv}$ and $F_{\rm vh}$ have fixed phases. We alleviate this assumption with the exact EM model that yields complex copolar and cross-polar radiation patterns. Starting with (1), the authors [13] relate the ensemble average of second-order voltage moments (powers and cross-correlation) to the ensemble averages of the second-order moments of the scattering coefficients, i.e., $\langle |s_{\rm hh}|^2 \rangle$, $\langle |s_{\rm vv}|^2 \rangle$, and $\langle s_{\rm hh}^* s_{\rm vv} \rangle$. It is customary to assume these moments are constant within the radar resolution volume. The integration over the resolution volume produces the powers for horizontal polarization $P_{\rm h}$ and vertical polarization $P_{v,}$ where Z_{dr} is differential reflectivity in linear scale, and $\rho_{\rm hv}$ is the copolar correlation coefficient. True differential

reflectivity (unbiased by radiation patterns F_{hh}=F_{vv}) is given by Z_{dr}=$<|s_{hh}|^2>$ / $<|s_{vv}|^2>$ and the copolar correlation coefficient is $\rho_{hv} = \frac{\langle s_{hh}^* s_{vv} \rangle}{\sqrt{\langle |s_{hh}|^2 \rangle \langle |s_{vv}|^2 \rangle}}$.

Starting from (1), we derive the powers in horizontal P_h and vertical P_v channels (3 a,b). The integrals are over a solid angle Ω, and integration along the range is omitted because it is constant, having no bearing on the variables. Note that these equations are exact in that they contain all the terms under the integrals, whereas the analogous pair of equations in ([13] eq. 9) lack third and fourth-order terms.

The differential reflectivity bias (δZ_{DR}) is estimated from (3a) and (3b), and on a logarithmic scale, it is

$$\delta Z_{DR} = 10 \log_{10}\left(\frac{P_h}{P_v}\right) - Z_{DR}, \tag{4}$$

where Z_{DR} (dB) is the true differential reflectivity.

To further illustrate, take the ratio (3a) to (3b) and consider only the integrals over the main copolar lobe patterns. The result is

$$\frac{P_h}{P_v} = Z_{dr} \frac{\int_\Omega |F_{hh}|^4 d\Omega}{\int_\Omega |F_{vv}|^4 d\Omega}. \tag{5}$$

The power's ratio will be biased if the ratio of integrals differs from 1. Conceptually this zero-order bias is easy to quantify if the two-way power patterns are known. These are the first and last terms in the eq. (3a, b), namely the $|F_{hh}|^4$ and $|F_{vv}|^4$. The contribution to bias by other terms from (3) is harder to quantify. Of these, the first-order cross-polar voltage patterns contribute the most, as the following relative contribution of the terms illustrates

$$\left|\int_\Omega |F_{hh}|^2 F_{hh} F_{vh}^* d\Omega\right| > \int_\Omega |F_{hh}|^2 |F_{hv}|^2 d\Omega > \left|\int_\Omega F_{hh} F_{hv} F_{vh}^{*\,2} d\Omega\right|. \tag{6}$$

The reference [13] lists the equivalent to equations (3) but without the third and fourth-order terms. For completeness and various comparisons, we keep all the terms and refer to ensuing solutions as exact. The expression of bias up to second-order terms, i.e., the first and second one from the left in (6), as well as similar ones in [13], is

$$\delta Z_{DR} = 10(A_1 + A_2) \log e, \tag{7}$$

where A_1 has F_{hv} raised to the first power (i.e., to first order) in the integrals, whereas F_{hv} to the second order appears in A_2. The two are (8a) and (8b), as shown at the bottom of the next page.

The differential reflectivity bias is then given by (7). Note that these equations contain phases of various patterns and that the approximation (8) with up to second-order terms was used for two purposes [13]: 1) to demonstrate that first-order bias terms cancel if cross-polar patterns have four axially symmetric equal lobes with respect to the main lobe's center; 2) to further approximate and simplify (8) and thus establish bounds on the bias as functions of Z_{DR}, ρ_{hv}, β, and other differential phases.

Further examination of (3) reveals that first-order bias terms also vanish if the cross-polar pattern has two lobes (within the main lobe) antisymmetric with respect to the principal plane. That occurs in patterns of the antenna pointed along either principal plane. To generalize findings in [13], if the cross-polar patterns have these two types of antisymmetric lobes, then the terms containing the cross-polar patterns to the first and third powers vanish. Specifically, in both equations (3), the 2nd, 4th, 5th, and 9th terms disappear. Moreover, in the approximate solution (8), $A_1 = 0$, A_2 remains with all the second-order terms (the higher-order terms are ignored).

For computing bias out of the principal planes, the first-order terms dominate; hence one can ignore A_2 and express the bias as

$$\delta Z_{DR} = 20 \log(e)\left\{W_{hv}\left[\cos(\beta) - \rho_{hv} Z_{dr}^{\frac{1}{2}} \cos(\beta)\right] - W_{vh}\left[\cos(\beta) - \rho_{hv} Z_{dr}^{-\frac{1}{2}} \cos(\beta)\right]\right\}, \tag{9}$$

where

$$W_{hv} = \int F_{hh}^3 |F_{hv}| d\Omega / \int F_{hh}^4 d\Omega, \tag{10a}$$

and

$$W_{vh} = \int F_{hh}^3 |F_{vh}| d\Omega / \int F_{hh}^4 d\Omega, \tag{10b}$$

are the antenna's bias weighting factors that measure the effectiveness of the cross-polar field in generating Z_{DR} bias. Hereafter we refer to (9) as "approximation," and it has been used in [13] to set bounds on the bias.

In summary, bias caused by the $|F_{hh}|^4$ term in P_h and $|F_{vv}|^4$ in P_v can be easily accounted for because the correction is a multiplying factor. And it may be the only needed correction if the contribution by the other terms is small. However, that depends on the cross-polar patterns. What matters most is the shape of these patterns within the main beam. The cross-polar patterns with symmetric lobes of the opposite sign within the main lobe would not bias Z_{DR}. But cross-polar pattern having a lobe coaxial with the copolar pattern's main lobe would cause significant bias. Similar bias could be caused by coupling between the H and V signals in the radar. Typically, PPAR's cross-polar patterns at the broadside have four symmetric lobes of opposite signs, but in the principal plane, these have two symmetric lobes of opposite signs.

The other polarimetric variable we investigate is the correlation coefficient ρ_{hv} between horizontally and vertically polarized returns. This variable is very useful for characterizing the quality of the radar system [19], [11]. Examining various system contributions to bias in ρ_{hv} can isolate the most contributing component. Here we analyze the contribution of mainlobe patterns mismatch and a mismatch in the pointing direction of the TPD. For that, we take equation (6) from [11] to express the bias parameter ξ.

$$\xi = \frac{\int F_{hh}^2 F_{vv}^2 d\Omega}{\left(\int F_{hh}^4 d\Omega\right)^{\frac{1}{2}} \left(\int F_{vv}^4 d\Omega\right)^{\frac{1}{2}}} \tag{11}$$

where $(1 - \xi)\rho_{hv}$ is the bias, and the pattern functions are as in (2). The integrals in (11) are over the solid angle encompassing the mainlobes. Formulation (11) addresses the correlation coefficient bias due to the mainlobe mismatch only,

assuming that cross-polar pattern contribution is negligible. However, following [14] we can derive the copolar correlation coefficient bias due to all terms of antenna radiation as:

$$\delta\rho_{hv} = \left(1 - \frac{\int_\Omega (V_h(t)V_h(r))^*(V_v(t)V_v(r))d\Omega}{\sqrt{\int_\Omega V_h^2(t)V_h^2(r)d\Omega}\sqrt{\int_\Omega V_v^2(t)V_v^2(r)d\Omega}}\right) \times \frac{\langle s_{hh}^* s_{vv}\rangle}{\sqrt{\langle|s_{hh}|^2\rangle\langle|s_{vv}|^2\rangle}}, \quad (12)$$

where $V_h(t,r)$ and $V_v(t,r)$ are given by (1), and integration is over the resolution volume Ω.

And finally, from the argument of the ρ_{hv} we can determine the differential phase bias, which is important for rainfall rate estimates [19]. The differential phase bias can be obtained as

$$\Delta\Phi_{DP} = \arg\left[\int_\Omega (V_h(t)V_h(r))^*(V_v(t)V_v(r))d\Omega\right] - \Phi_{DP}, \quad (13)$$

where Φ_{DP} is a true differential phase due to propagation and backscattering.

Having a physical model whereby phases across the patterns within the main lobe are known enables assessing pattern effects on polarimetric variables' bias. This is especially important for PPARs, whereby the patterns differ at every pointing direction. Also, with the exact formulation exemplified by solving (3), we can evaluate how good is the second-order approximation for differential reflectivity bias and find the copolar correlation coefficient bias due to miss-matched mainlobes. Moreover, we may determine if these approximations are sufficiently accurate to gauge data quality at the pointing direction where the odd symmetry of cross-polar patterns does not hold.

Next, we explain modeling the patterns of the TPD. Specified biases of radar variables [20] we listed in Table I.

TABLE I
BIAS IN RADAR VARIABLES SPECIFIED BY NATIONAL WEATHER SERVICE (NWS) [20]

Reflectivity	1 dBZ for scatterers with spectrum width 4 m s^{-1} and SNR > 10 dB
Velocity	0.0 m s^{-1} for scatterers with spectrum width 4 m s^{-1} and SNR > 8 dB
pectrum Width	0.2 m s^{-1} for scatterers with true spectrum width of 4 m s-1 and SNR >10 dB
Differential Reflectivity	0.1 dB for scatterers with differential reflectivity (Z_{DR}) of less than ±1 dB, spectrum width 2 m s^{-1}, Correlation Coefficient ≥ 0.9, dwell time 50 ms, and SNR ≥ 20 dB; for Z_{DR} with a magnitude greater than 1 dB, bias should be less than 10% of Z_{DR}
Correlation Coefficient	0.006 for scatterers with spectrum width 2 m s^{-1}, Correlation Coefficient ≥ 0.99, dwell time 50 ms and SNR ≥ 20 dB
Differential Phase	1° for scatterers with spectrum width 2 m s^{-1}, Correlation Coefficient ≥ 0.99, dwell time 50 ms and SNR ≥20 dB

TABLE II
LIST OF TPD CHARACTERISTICS

Table 2. List of TPD Characteristics	
Mode	Pulse compression
Frequency	2.87 GHz
Peak transmit power	3 kW
Compression ratio	10
Compressed pulse	2 μs
Linear FM Δf	330 kHz
Weighting	Uniform
PRT nominal	1 ms
Number of pulses	128
Beamwidth	Az=6.3° ; El = 2.5°
Mainlobe match	2 dB at – 20 dB
Cross-polar pattern	-45 dB below copolar peak

III. RADAR ANTENNA AND ITS MODEL

A. Radar Antenna

The TPD (Fig. 1) was meant to serve as proof of concept; hence it has rudimentary properties. Its characteristics are listed in Table II.

The three last rows specify the antenna performance. The antenna consists of ten panels in a 2×5 matrix, and each panel contains 8×8 patch radiators spaced at half wavelength. For transmission, panels radiate independently. For the reception, the panels are combined into eight overlapping subarrays, each consisting of two panels (Fig. 2). Therefore, there are 16-time series (I, Q), eight for each polarization. These are recorded for further processing as the radar has no real-time capability. The antenna is mounted on a trailer.

The reason for our choice is to have a basic radar with a sufficiently large antenna to get an idea about performance issues that may be facing a larger PPAR antenna. The antenna can be oriented vertically with its larger axis (dimension) in the vertical plane or its smaller axis in the vertical plane. The former orientation is advantageous for quick testing and

$$A_1 = \frac{2\int_\Omega |F_{hh}|^2 Re\left\{F_{hh}^* F_{hv} e^{j\beta} - F_{hh}^* F_{vh} e^{-j\beta} + \rho_{hv}\left[e^{-j\Phi_{DP}}(Z_{dr}^{-\frac{1}{2}} F_{hh} F_{hv}^* e^{j\beta} - Z_{dr}^{\frac{1}{2}} F_{hh}^* F_{vh} e^{-j\beta}\right]\right\} d\Omega}{\int_\Omega |F_{hh}|^4 d\Omega}, \quad (8a)$$

$$A_2 = \frac{\int_\Omega |F_{hh}|^2 \left\{|F_{hv}|^2 - |F_{vh}|^2 + Z_{dr}^{-1}|F_{vh}|^2 - Z_{dr}|F_{hv}|^2 + 2\rho_{hv} Re\left\{e^{-j\Phi_{DP}}\left[Z_{dr}^{-\frac{1}{2}}(F_{vh}^{*\,2} + F_{hv}F_{vh}^*\right] - Z_{dr}^{\frac{1}{2}}\left(F_{hv}^2 + F_{hv}F_{vh}^*\right)\right\}\right\} d\Omega}{\int_\Omega |F_{hh}|^4 d\Omega}. \quad (8b)$$

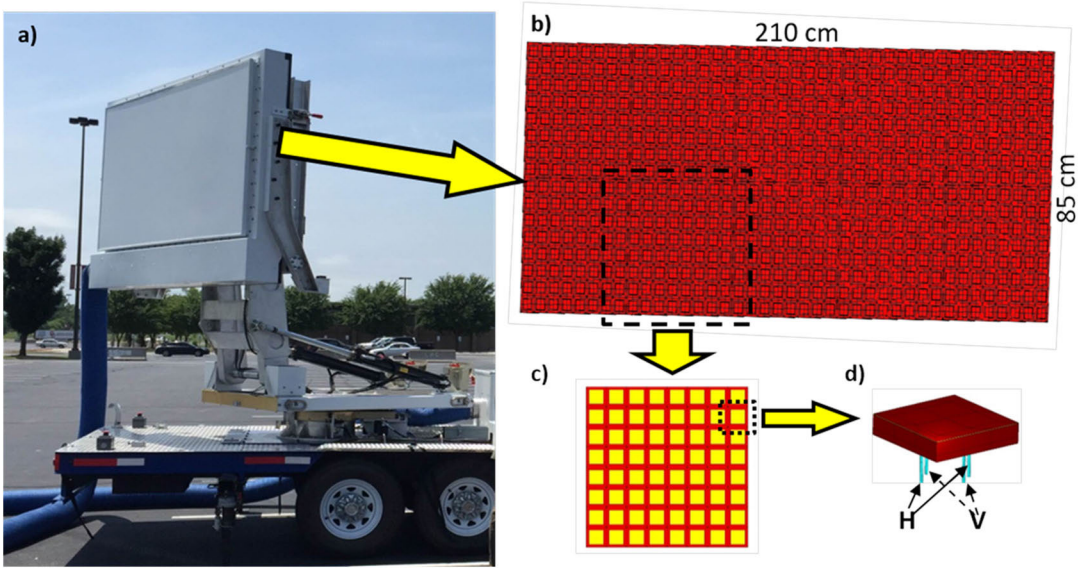

Fig. 1. a) The Ten Panel Demonstrator radar; b) the antenna model; c) antenna panel; d) the antenna element with four differentially fed probes.

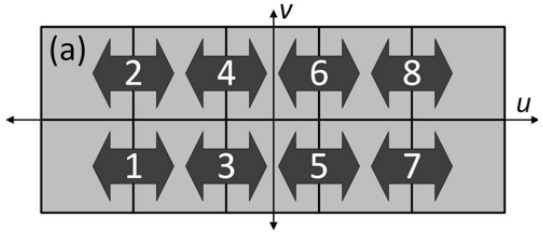

Fig. 2. Arrangement of panels and subarrays on the TPD. The subarrays are numbered from 1 to 8. On transmission, all panels comprise a single antenna. On reception, an analog beamformer combines signals from adjacent panels into an overlapped two-panel subarray structure. Arrows and numbers indicate which panels form each of the eight subarrays are combined. Adapted from [21].

assessment of performance from scans in elevation (RHI). This is because, in that configuration, the beam is narrower in the vertical (elevation) direction and, therefore can resolve the vertical structure of precipitation. Specifically, the vertical structure varies significantly from below to above the melting layer in horizontal uniform stratiform precipitation. This causes known variations in the polarimetric variables, which can be a useful standard for evaluating radar performance. The lateral (azimuthal) structure of precipitation is relatively uniform and hence would not affect measurements with the wide lateral beam.

The TPD can transmit linear H and V polarized fields in succession from pulse to pulse or simultaneously (SHV). The latter is the preferred polarimetric mode on weather radars and is the one operating on the WSR-88Ds. In the SHV mode, coupling between the two polarized signals is strongest as each copolar component couples into the cross-polar, strongly affecting the returns of the orthogonal component. The biggest challenge for this mode is achieving sufficient isolation between copolar and cross-polar components. In the alternate polarimetric mode, coupling effects are significantly reduced because the orthogonal channel, wherein the strongly coupled component returns, is not processed.

B. Antenna Model

The TPD model is created using the WIPL-D software [18]. The antenna has two axis of symmetry, which can be exploited in modeling its geometry. In WIPL-D software the antenna is decomposed into four separate models for conducting one generator at the time (OGAT) analysis while the remaining generators are short-circuited. In these four simulations, the geometrical symmetry is substituted with Perfect Electric Conductor (PEC) and Perfect Magnetic Conductor (PMC) planes creating symmetry/anti-symmetry planes. Superimposing the results of these four simulations, WIPL-D calculates the final (whole array) radiation pattern. This approach yields the same results as the analysis of the full array without taking the array's geometrical symmetry into account [22], [23]. The main advantage of applying this method to large array simulation is lowering the necessary computer resources by about 16 times and therefore increasing the computational speed by up to about 16 times. The approach is designed to enable simulating true radiation of large geometrically symmetric structures [22], [23].

The antenna model supports electronic beam steering by changing the phase of the excitation ports on the element level. Patterns are separately simulated for H and V polarization. When simulating H polarization, antenna feeds for V polarization are load-matched and vice versa.

A comparison of simulation with measured results and a detailed description of simulating the panel are in [17]. We have established the one-panel cross-polar patterns agree very well with the measurements [17]. This boosts confidence in the model of the full array antenna. Our interest in discrepancies between measured and simulated patterns comes from the paucity of available studies that relate manufacturing errors in patch antennas to the polarimetric variables. Available studies of radiation pattern degradation due to surface errors in reflector antennas [24], [25], [26], which we expect to produce similar effects as manufacturing errors in horizontal

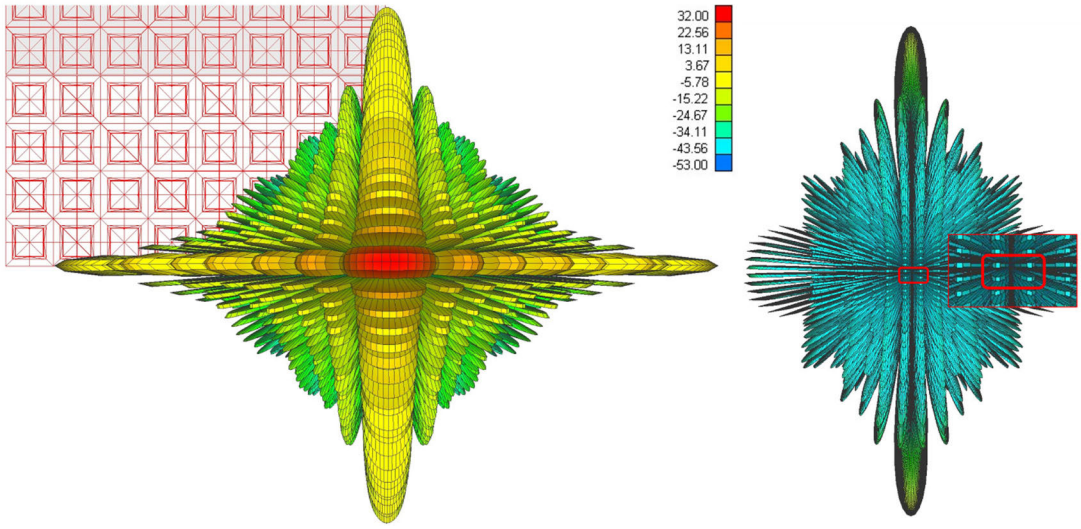

Fig. 3. Broadside copolar and cross-polar patterns of the TPD radar. The left image shows the copolar pattern; the right image contains the cross-polar pattern with four zoomed-in lobes symmetric around the origin. These lobes are more than 70 dB lower than the copolar peak. The minimum in the cross-polar patterns is at the beam center, and it is lower than -100 dB.

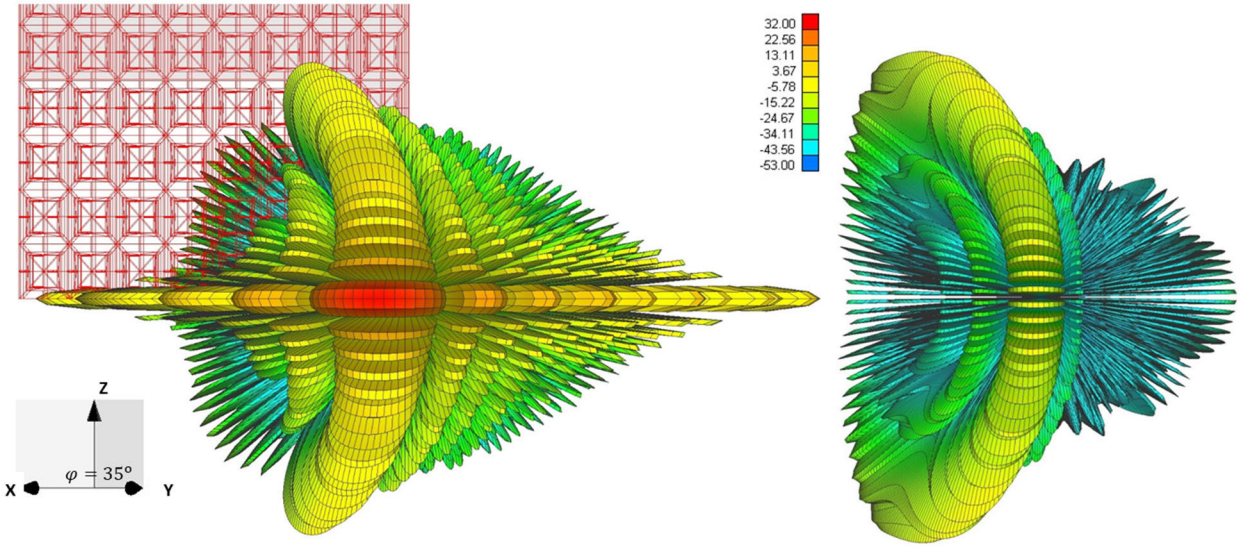

Fig. 4. Copolar and cross-polar radiation patterns of the TPD electronically steered to 35° away from the broadside in azimuth. The copolar pattern (left) and its corresponding cross-polar pattern (right). The cross-polar pattern exhibits two lobes of the opposite sign within the main love; these are over 35 dB lower than the copolar peak, and the null between these two lobes is at least 100 dB smaller than the copolar peak.

patch antenna dimensions, suggest a relation between the manufacturing error and decrease of cross-polar isolation. The tolerances given for the manufacturing process employed in making the TPD antenna are substantially smaller than 0.01λ, and following the formulations derived for reflector antennas [21] we expect the degradation in isolation between the copolar and cross-polar patterns to be smaller than our cross-pol peak levels.

Concerning the construction of the antenna from panels, reference [10] states that random additions of bias contributions from panel to panel cause acceptable errors in the correlation coefficient of the specific panel design. But coherent addition causes unacceptable bias in the correlation coefficient. It is highly unlikely that all panels would have identical flaws; hence the incoherent addition is expected in practice.

The simulation results of the broadside exhibit the expected characteristics of the copolar and cross-polar patterns (Fig. 3). The four axially symmetric cross-polar lobes are within the main copolar lobe. This feature is present in the patterns of the WSR-88D [13]. The four cross-polar lobes have alternating opposite phases; thus, their contribution to the first-order and third-order bias vanishes (terms containing β). This results in lower bias values, as presented in the following section.

When the beam is electronically steered away from the broadside but in the principal (horizontal) plane, the copolar main lobe widens, and copolar sidelobes become asymmetric. The cross-polar lobes change from four axially symmetric to two symmetric with respect to the azimuthal plane (Fig. 4). These cross-polar lobes have opposite phases, and their contribution also cancels the first and third-order bias terms.

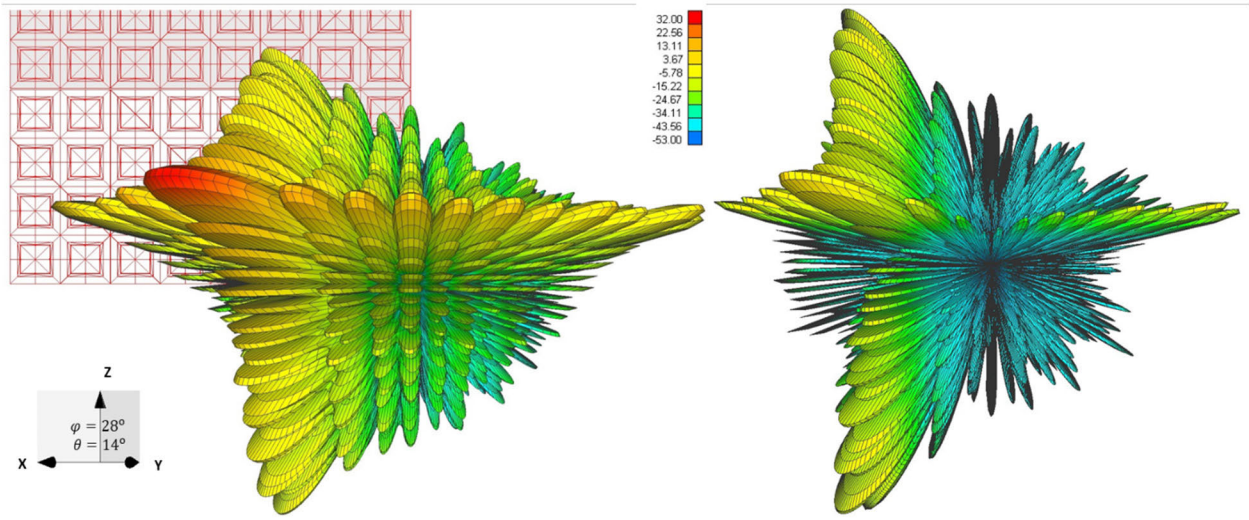

Fig. 5. Copolar and cross-polar radiation patterns of the TPD radar electronically steered 28° out of broadside in azimuth and 14° in elevation. The main copolar lobe (left) and the main cross-polar lobe (right) are prominent. The cross-polar lobe is 24 dB lower than the copolar main lobe and has a peak-to-peak angular offset of 1° in azimuth and 0.5° in elevation.

For the beam steered out of the principal planes to ϕ = 28°; θ = 14° the radiation patterns are plotted in Fig. 5. It is significant (not easy to see) that the position of the main copolar lobe is offset from the steered one to ϕ= 28.5°;θ = 12.5°. This must be known to account for in electronic beam steering and to quantify Z_{DR} bias. The cross-polar lobe is now within the main copolar lobe. The maxima of the two lobes are offset by 1° in azimuth and −0.5° in elevation. Clearly, the cross-polar lobe would cause first-order bias to the polarimetric variables because it does not have a twin lobe of the opposite sign to cancel. This occurs in directions out of the principal planes and is referred to as geometrically induced bias. To avoid this bias pulse to pulse phase coding has been proposed [27], [28], [29], and effectiveness has been proven on recorded time series data [30]. Nonetheless, to this date, a successful quantified correction in real time has yet to be demonstrated.

The difference between copolar and cross-polar peak gain (cross-polar isolation) in the H patterns (Fig. 5) is 24.4 dB, and in the V patterns, it is 25.7 dB (one-way). The phase differences between the copolar and cross-polar lobes are 22.5° for H-polarization and 153.5° for V-polarization. The phase difference between the two copolar lobes is $1^{o,}$ and between the cross-polar lobes, it is 132.2°. All these phases are average values and variations within the lobes are up to about 10°. Therefore, approximations and guesses, as in [13], are inadequate to gauge antenna-induced bias in the polarimetric variables. Full EM models are a more realistic option for this purpose.

With the calculated antenna patterns, we evaluate the biases using eq. (4) and (12). For differential reflectivity bias, we use the full solution (4), the 2nd order approximation (7), as well as a further "approximate" formula (9) for comparison. These comparisons can establish the validity of the second-order approximation (8) and its "approximate" form (9). This also limits the contribution of the higher-order terms [13]. The copolar correlation coefficient bias calculated using (12) is compared to the main beam mismatch bias formulation (11).

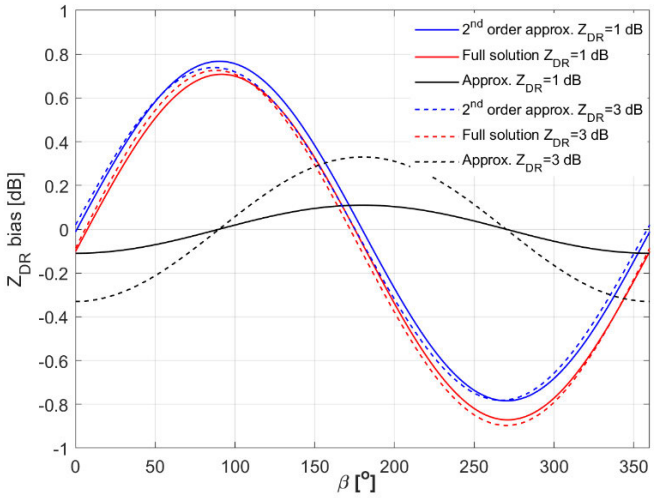

Fig. 6. Differential reflectivity bias caused by the antenna radiation patterns' dependence on the transmission differential phase. The intrinsic Z_{DR} is listed, the assumed ρ_{hv}= 0.99, and Φ_{DP} = 0°. The antenna is pointing at ϕ = 28°, θ_e = 14°.

Next, we illustrate bias for specific intrinsic Z_{DR} of 1 dB and 3 dB and ρ_{hv} of 0.99. The chosen Z_{DR}s are within a range for rain or dry snow, and so is ρ_{hv} = 0.99 [31]. We assume the total differential phase Φ_{DP} is zero; at other values, the bias curve would change phase and amplitude with respect to the β axis. The desired bias for Z_{DR} < 1 dB is 0.1 dB, and for larger Z_{DR} values is $0.1Z_{DR}$. We plot the bias as a function of the differential phase (β) between the two transmitted fields. Following from the patterns, it is obvious that steering out of the principal planes and having a collocated cross-polar peak is the worst-case scenario in terms of Z_{DR} bias. As biases for antenna pointed broadside or in the principal planes are lower, we show, for comparison, the bias for a pointing direction out of the principal planes in Fig 6.

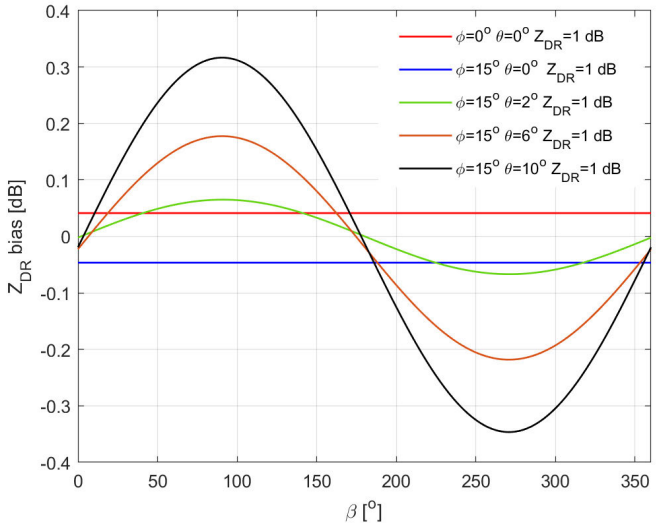

Fig. 7. The differential reflectivity bias caused by the antenna radiation patterns' dependence on the elevation angle. The intrinsic Z_{DR} is listed, the assumed $\rho_{hv} = 0.99$, and $\Phi_{DP} = 0°$. The antenna is pointing at $\phi = 15°$.

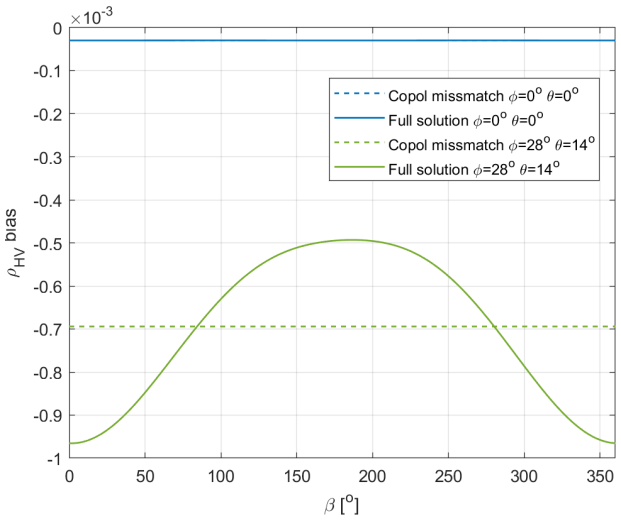

Fig. 9. The copolar correlation coefficient bias caused by the transmitted differential phase β. The intrinsic $Z_{DR} = 1$ dB, the assumed $\rho_{hv} = 0.99$, and Φ_{DP} =0°. The antenna is pointing at broadside and $\phi = 28°$, θ_e =14°.

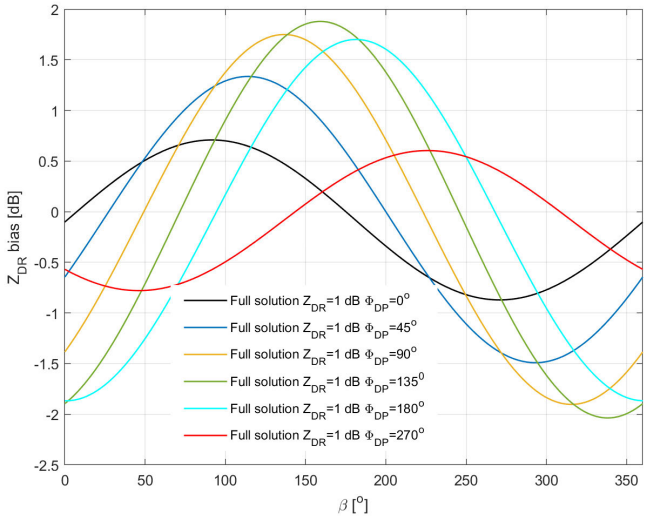

Fig. 8. The differential reflectivity bias caused by the transmitted differential phase β. The intrinsic $Z_{DR} = 1$ dB, the assumed $\rho_{hv} = 0.99$, and Φ_{DP} changes in steps of 45°. The antenna is pointing at $\phi = 28°$, θ_e =14°.

We consider two representative cases: Z_{DR} of 1 dB and 3 dB. Biases computed from the full solution (4) and 2nd order solution (7) closely follow each other. The important difference is the zero bias for β= 0° exhibited with the 2nd−order solution. The full solution estimates close to -0.1 dB bias. The maximal difference between the two solutions is less than 0.08 dB. We see out of the principal planes. The bias is larger than 0.1 dB for most β regardless of which of the two Z_{DR}s is measured. The "approximate" solution is inaccurate in both bias amplitude and phase. It can't be used for quantitative evaluation of similar PPAR antennas.

Next, we use the full solution (4) to determine the Z_{DR} bias for a few pointing directions (Fig. 7). At broadside, the bias is about 0.04 dB for $Z_{DR} = 1$ dB. Broadside bias is independent of the Z_{DR} value, as the second term (bracket) in the P_h and P_v is zero. At 15° azimuth in the principal plane, the bias is -0.05 dB. With increasing elevation, the peak bias increases so that at $\theta = 10°$, it is a tad over 0.3 dB. Bias also increases with increasing azimuth to reach -0.1 dB at 35° azimuth and 0° elevation (not shown).

Our calculations/simulations consider antenna cross-polar radiation and geometrically induced biases (non-orthogonal transmission and geometrical deviation), whereas system bias is not considered. Therefore, Fig. 6 is applicable for relative comparisons. To determine the worst-case bias, one must consider $\Phi_{DP,}$ as explained next.

We assume the beam pointing is the same as in Figure 5. With increasing $\Phi_{DP,}$ Z_{DR} bias using the full solution (4) rises to reach a maximal absolute value of 1.88 dB at $\Phi_{DP} = 135°$, $\beta = 159°$ (Fig. 8). Besides the increase of the minimal and maximal value, the bias's dependence on β shifts proportionally to the increase of Φ_{DP}. This is caused by the real part of the second term in H and V powers (3a, 3b), which is affected by the differential phase. Because such a large bias is unacceptable, mitigation methods have been proposed. One is pulse-to-pulse phase coding on transmission and spectral processing on reception to eliminate the strongly coupled component [28], [32]. That technique eliminates the first and third-order contribution by the cross-polar patterns to Z_{DR} bias similar to the AHV polarimetric mode. Time-multiplexing has also been proposed [28] and is equivalent to the AHV mode in eliminating the first and third-order bias. Further investigation of time multiplexing indicated that the reflectivity gradients in range and antenna gain mismatch might diminish the efficiency of the approach [29]. To our knowledge, no methods can neutralize the second-order bias in polarimetric variables regardless of the polarimetric mode.

A previous study using the TPD radar [34], among other issues, considers the Z_{DR} bias. In light of the results presented here, their findings of Z_{DR} bias are higher than measured, most likely due to the computational approach in modeling the radar array antenna. The authors [34] present results (Fig.3 c, e) that

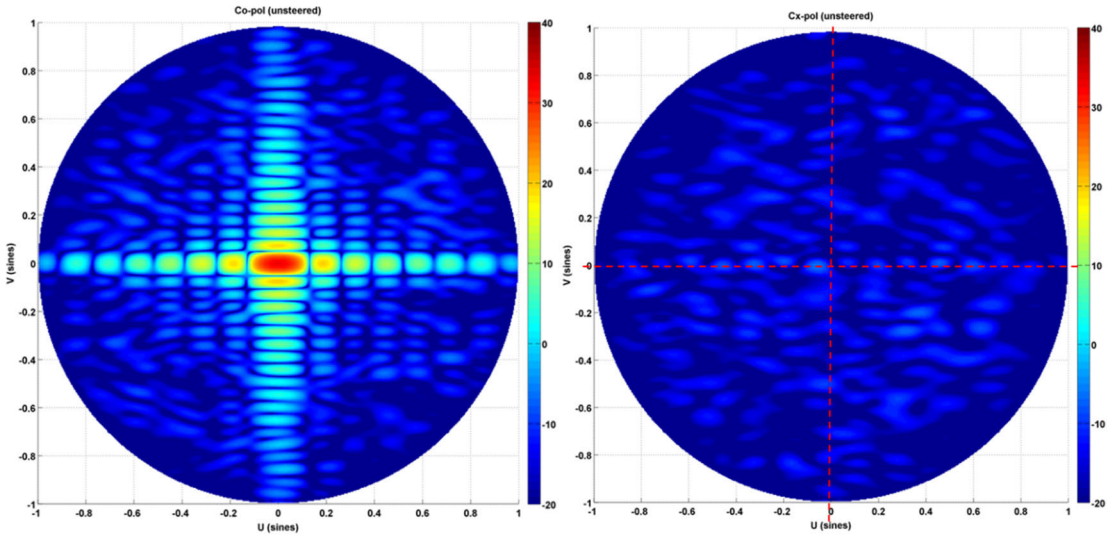

Fig. 10. Ten Panel Demonstrator copolar (left) and cross-polar (right) radiation pattern at broadside calculated using the infinite array method in HFFS software. The color bar indicates dBi, and the red dotted lines are added to the cross-polar pattern to facilitate reading [9].

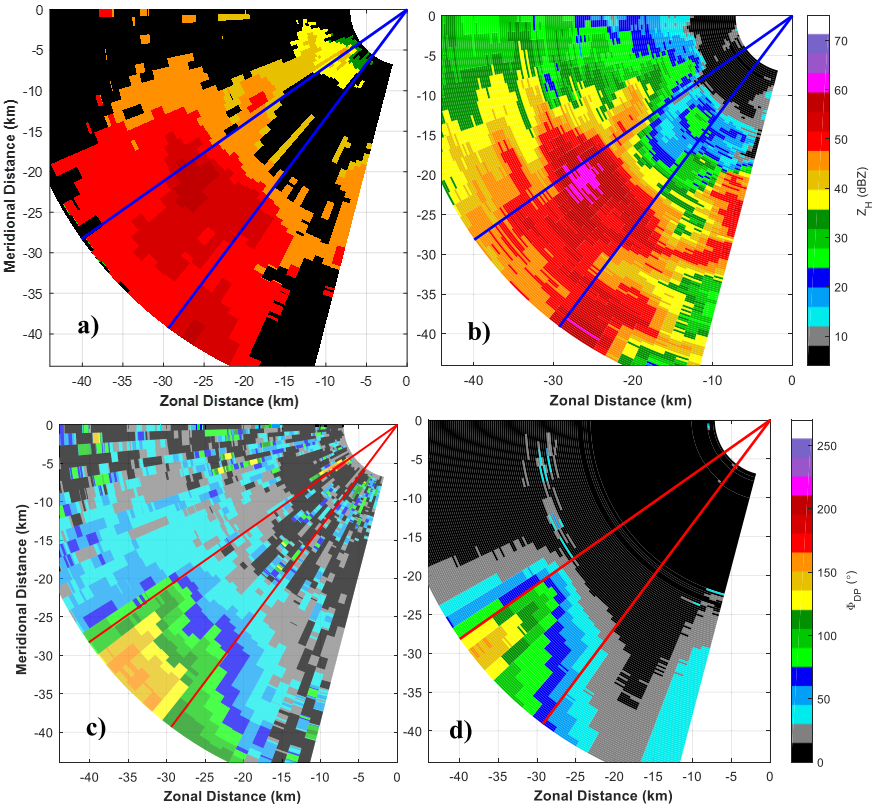

Fig. 11. (a) Reflectivity field over a sector scanned with the TPD at elevation equal 1°. (b) Same as (a), but with the KOUN at elevation equal 1.8° (c) Differential phase field over a sector scanned with the TPD radar at elevation 1°. (d) Same as (c), but over a sector scanned with the KOUN radar at elevation 1.8°. Scans made at 1759 UTC, on 15 May 2018.

fail to exhibit the lobe structure of the cross-polar patterns, possibly causing overestimation of Z_{DR} bias for azimuth of $\pm 35°$(1.25 dB simulated compared to -0.2 dB and 0.5 dB measured, ([34] Fig. 5 a). We submit that cross-polar pattern simulation using the approximate technique authors used may be inadequate for assessing the calibration of polarimetric phased array radars. When the study [34] was made, we had not yet developed the model described herein.

In addition to differential reflectivity bias, we evaluate copolar correlation coefficient bias for the two cases resulting in the lowest and highest Z_{DR} bias. The copolar correlation coefficient bias is calculated assuming only the copolar mainlobe effects (11) and considering both the copolar and cross-polar patterns as in (12). The copolar mismatch bias (Fig. 9) equals to about the median value of the bias calculated using the full solution (12). The full solution variation is

TABLE III
SIMULATION TIME FOR A SINGLE PANEL WITH ONE EMBEDDED ELEMENT EXCITED FOR BOTH POLARIZATIONS FOR EACH SOLVER

	WIPL (MoM)[1]	CST (Transient)[2]	HFSS (FEM)[3]
Time	3h 20min	5h 30min	>6h

[1]Method of moments. [2]Time domain solution. [3]Finite element method.

caused by β changing the phase of the cross-polar pattern. Another interesting conclusion can be drawn from Fig. 9; the cross-polar radiation contribution to the correlation coefficient bias evaluated using the full solution is negligible for the broadside case (dashed and solid blue curves overlap). This is the same as in the bias of differential reflectivity whereby the contributions by the four cross-polar lobes cancel out.

Models of the TPD antenna, presented here, take about 50 hours per polarization and a pointing direction to simulate in the WIPL-D CEM solver.

C. Simulation of a Single Panel

We have tested different numerical methods for simulating TPD's single panel to compare simulation times and method accuracies. We present the simulation time comparison for brevity, whereas a more detailed evaluation is in [17]. We compare the simulation times of the following three solvers: HFSS, CST, and WIPL-D. Simulations are carried out on an Intel i7 processor with 32GB of RAM. The model was of a single panel with one central element excited, and the rest load matched. The results are in Table III.

D. Approximate Techniques for PAR Antenna Simulation

Assessing the simulation results obtained using an approximate technique was done by the HFSS (infinite array) solver. Results are presented in Fig. 10. The copolar main lobe is well-defined. In contrast, sidelobes in the vertical principal plane and out of principal planes exhibit unexpected variations and lack of symmetry. The results from the approximate technique simulation of the cross-polar patterns are worse. Contrary to the symmetric cross-polar lobes around the origin we obtained from WIPL-D simulations, the cross-polar lobe structure in the center is not symmetric. Furthermore, it seems that the infinite array technique has underestimated cross-polar isolation. The peak-to-peak isolation in the WIPL-D results is about 80 dB, whereas it is about 40 to 50 dB in the infinite array results.

Overall approximate techniques may be sufficient for determining the beamwidth and shape of the copolar pattern and the first few sidelobes. However, the application where far sidelobes and cross-polar radiation are needed is limited and may not be sufficiently accurate for use in polarimetric calibration.

IV. WEATHER OBSERVATIONS USING TPD

To determine if TPD could function as a polarimetric radar, we collected some data and compared these with data from a collocated research WSR-88D designated as KOUN. The data have been recorded almost simultaneously (within 59 s) by both radars. The TPD collected time series data (8 streams of I, Q at H polarization and eight streams at V polarization) at elevations 1° and 2°. The recorded TPD's azimuth and range locations have high relative precision but unknown absolute reference. To establish the absolute pointing direction and range locations, we compared the fields of differential phases from the KOUN and TPD and made adjustments to the coordinates of the TPD data. The range and azimuth steps, as well as the beam widths, differ on these radars [35]. Therefore, on KOUN data, we applied an 11-point mean filter (5.5°) in the azimuth direction and plotted data at 2° increments. We used a 42-range-point median filter (2015 meters) for each TPD's radial of data.

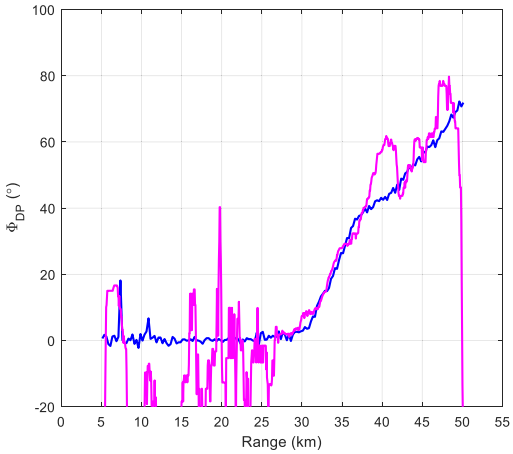

Fig. 12. Radial profiles of the differential phase: from the TPD's data at elevation 1°, azimuth 216.5° (pink graph) and from the KOUN's data at elevation 1.8°, azimuth 216.8° (blue graph).

The TPD's hardware has instabilities related to temperature and system synchronization. Therefore, precise measurements of differential reflectivity and correlation coefficient were not possible. Nonetheless, measurements of reflectivity and differential phase are little affected by these issues and hence are presented. Figs. 11 a and 11 b depict the fields of Z_H measured by the TPD (Fig. 11 a), and KOUN (Fig. 11 b) radars on conical sector scans at 1° elevation (for the TPD radar) and 1.8° elevation (for the KOUN radar). The precipitation band is characterized by high Z_H (exceeding 55 dBZ). Comparing Figs. 11 a and 11 b between 2 blue solid lines, we notice a similar shape of the area with high values of Z_H. The TPD's reflectivity factor Z_H is about 2 dB lower and overwhelmed by noise for Z_H smaller than 35 dBZ at a distance from the radar larger than 10 km compared to the KOUN's reflectivity factor. This is explained by the large beamwidth (incomplete beam filling results in lower Z values) and significantly lower TPD detectability.

The fields of the differential phase from the TPD are in Fig. 11 c, and from the KOUN, they are in Fig. 11 d. The fields are fairly similar in patterns and values. The Φ_{DP} pattern from TDP is broader, likely because its beam cross section is much larger (about 12 times the one of KOUN). Therefore, it samples precipitation from a wider span of altitudes than the KOUN. Depending on the vertical profile of reflectivity, the beam-weighted values can be larger or smaller. What matters are the Φ_{DP} radial gradients. These are comparable.

For example, we plot the radial profiles at 216.5° in azimuth (Fig. 12). At a range beyond about 37 km, the Φ_{DP} of TPD exhibits nonmonotonic increase likely due to nonuniform beam filling and possibly backscatter differential phase from regions illuminated by the wide TPD beam but not by the much narrower KOUN beam. The good agreement from about 25 to 37 km confirms the robustness of phase measurement discussed in section III. Therefore, along this range, rainfall can be measured via the $R(K_{DP})$ relations or from specific attenuation [19]. In addition, compensation of reflectivities for attenuation is feasible.

V. Conclusion

We have presented results from EM modeling of antenna patterns on the Advanced Technology Demonstrator proof of concept phased array weather radar called Ten Panel Demonstrator. Although the model uses commercial software, it needs human interaction and detailed knowledge of radiators to set it up. The antenna size is 2.1 × 0.8 m and, to our knowledge, is the largest PAR antenna for weather applications on which a full simulation model of the sort had been applied. Our model yields copolar and cross-polar patterns needed to estimate bias in polarimetric variables.

We focus on the SHV mode of polarimetric generation/processing because it has smaller errors in polarimetric variables' compared to the AHV mode. Magnitudes and phases of antenna patterns establish bias in the polarimetric variables.

The model confirms that cross-polar patterns within the main pattern lobe have four axially symmetric lobes of the alternating sign at the broadside. The cross-polar patterns from pointing directions in the principal planes have two lobes of opposite signs. These features make the differential reflectivity and correlation coefficient bias independent of the cross-polar pattern to the first and third order but dependent on the second and fourth order. Therefore, the peak copolar to cross-polar power ratio as low as 25 dB is sufficient to constrain Z_{DR} bias within the desired range of ±0.1 dB. Otherwise, twice as large cross-polar system isolation (antenna and radar combined) is needed to control the bias. If beams are pointed in the principal planes, there is no need to apply special signal designs and/or processing to constrain bias.

What matters is the polarimetric mode of the radar and the shape of the cross-polar patterns within the main lobe pattern. In the alternate polarimetric mode, acceptable bias can be achieved with one-half (in dB) of the copolar to cross-polar power ratios.

The bias in the polarimetric variables due to patterns within the mainlobes in the case of conformal arrays can be computed via CEM analogously as for planar arrays. This would be done by specifying the conformal arrays' physical layout in the WIPL-D software. From computed copolar and cross-polar patterns, various biases can then be estimated.

Although approximate techniques where radiation patterns of an individual element are combined with the array factor replicate well the copolar patterns, they are deficient for computing the cross-polar patterns. Moreover, the EM model results of the cross-polar pattern may be closer to the true pattern than the measured one once all measurement issues are considered.

The examples we chose are broadside patterns, patterns in a principal plane, and patterns out of the principal planes. We show the full antenna model of the TPD produces main lobe patterns in agreement with measurements. Moreover, we can determine an offset in the pointing directions between the peaks of the copolar and cross-polar patterns out of the principal planes. This is very hard to uncover in the field.

Precise measurements of differential phase and correlation coefficient were not possible due to instabilities caused by temperature and synchronization issues. The reflectivity and differential phase are much less affected; hence we compared these measured with the TPD to the ones measured with a collocated research WSR-88D. As expected from theoretical considerations, these agreed fairly well, implying that quantitative rainfall estimates using differential phase and reflectivity would be good.

The TPD served its purpose in that a large PPAR with identical panels can be constructed to advance this research further. Indeed, the Advanced Technology Demonstrator (1.6° by 1.6° beamwidth) has been built and is undergoing meteorological evaluations.

Acknowledgment

Igor R. Ivić made suggestions that have improved the manuscript. Branko Kolundžija provided extended insight about theoretical background of large antenna array modeling. The authors would like to thank the reviewers for meticulously examining the manuscript and providing valuable comments.

References

[1] D. S. Zrnic et al., "Agile-beam phased array radar for weather observations," *Bull. Amer. Meteorological Soc.*, vol. 88, no. 11, pp. 1753–1766, Nov. 2007.

[2] J. E. Stailey and K. D. Hondl, "Multifunction phased array radar for aircraft and weather surveillance," *Proc. IEEE*, vol. 104, no. 3, pp. 649–659, Mar. 2016.

[3] C. Fulton, M. Yeary, D. Thompson, J. Lake, and A. Mitchell, "Digital phased arrays: Challenges and opportunities," *Proc. IEEE*, vol. 104, no. 3, pp. 487–503, Mar. 2016.

[4] G. Zhang, R. J. Doviak, D. S. Zrnić, R. Palmer, L. Lei, and Y. Al-Rashid, "Polarimetric phased-array radar for weather measurement: A planar or cylindrical configuration?" *J. Atmos. Ocean. Technol.*, vol. 28, no. 1, pp. 63–73, Jan. 2011.

[5] G. Zhang, R. J. Doviak, D. S. Zrnic, J. Crain, D. Staiman, and Y. Al-Rashid, "Phased array radar polarimetry for weather sensing: A theoretical formulation for bias corrections," *IEEE Trans. Geosci. Remote Sens.*, vol. 47, no. 11, pp. 3679–3689, Nov. 2009.

[6] D. Mirković and D. S. Zrnić, "Polarimetric weather radar calibration by computational electromagnetics," *Appl. Comput. Electromagn. Soc. J.*, vol. 34, no. 2, pp. 342–346, Feb. 2019.

[7] M. Weber et al., "Towards the next generation operational meteorological radar," *Bull. Amer. Meteorological Soc.*, vol. 102, no. 7, pp. 1357–1383, Jul. 2021.

[8] V. M. Melnikov and D. S. Zrnić, "On the alternate transmission mode for polarimetric phased array weather radar," *J. Atmos. Ocean. Technol.*, vol. 32, no. 2, pp. 220–233, Feb. 2015.

[9] R. Palmer et al., "A primer on phased array radar technology for the atmospheric sciences," *Bult. Amer. Meteo. Soc. (BAMS)*, vol. 103, no. 10, pp. 2391–2416, 2022.

[10] D. Zrnic, D. Schvartzman, J. D. D. Díaz, R. D. Palmer, and A. Ryzhkov, "Effects of Horus antenna patterns on polarimetric weather observations," in *Proc. IEEE Int. Symp. Phased Array Syst. Technol. (PAST)*, Oct. 2022, pp. 1–7.

[11] D. S. Zrnic, D. Schvartzman, R. D. Palmer, and A. V. Ryzhkov, "Effects of Horus antenna patterns on the copolar correlation of weather returns," *IEEE Trans. Radar Syst.*, vol. 1, pp. 282–294, 2023.

[12] R. D. Palmer et al., "Horus—An all-digital phased array weather radar developed at the University of Oklahoma," in *Proc. 103rd AMS Annual Meeting*, Denver, CO, USA, 2023.

[13] D. Zrnić, R. Doviak, G. Zhang, and A. Ryzhkov, "Bias in differential reflectivity due to cross coupling through the radiation patterns of polarimetric weather radars," *J. Atmos. Ocean. Technol.*, vol. 27, no. 10, pp. 1624–1637, Oct. 2010.

[14] M. Galletti and D. S. Zrnic, "Bias in copolar correlation coefficient caused by antenna radiation patterns," *IEEE Trans. Geosci. Remote Sens.*, vol. 49, no. 6, pp. 2274–2280, Jun. 2011.

[15] F. Boldissar and A. Haile, "A near field measurement errors due to neglecting probe cross-polarization," in *AMTA Symp. Dig.*, St Louis, MO, USA, 2007.

[16] A. C. Newell, "Error analysis techniques for planar near-field measurements," *IEEE Trans. Antennas Propag.*, vol. 36, no. 6, pp. 754–768, Jun. 1988.

[17] D. Mirkovic and D. S. Zrnic, "Computational electromagnetic tools applied to the polarimetric phased array antenna," Nat. Severe Storms Lab. (NOAA), Norman, OK, USA, Tech. Rep., 2019.

[18] *WIPL-D*, WIPL-D d.o.o, Belgrade, Serbia, Dec. 2022.

[19] A. V. Ryzhkov and D. S. Zrnic, *Radar Polarimetry for Weather Observations*. Cham, Switzerland: Springer, 2019.

[20] *Radar Functional Requirements*, NOAA/NWS, Washington, DC, USA, 2015.

[21] I. R. Ivic, "On the polarimetric variable improvement via alignment of subarray channels in PPAR using weather returns," *IEEE Trans. Geosci. Remote Sens.*, vol. 59, no. 3, pp. 2015–2027, Mar. 2021.

[22] B. Kolundzija, D. Olcan, D. Zoric, and S. Stevanetic, "Efficient full wave 3D EM modeling of large phased arrays (by WIPL-D software)," in *Proc. IEEE Int. Symp. Antennas Propag. (APSURSI)*, Spokane, WA, USA, Jul. 2011, pp. 2732–2735.

[23] A. Sabouni, M. Ostadrahimi, S. Noghanian, and M. Pavlovic, "Three-dimensional accurate modeling of the microwave tomography imaging system," in *Proc. IEEE Int. Symp. Antennas Propag. (APSURSI)*, Spokane, WA, USA, Jul. 2011, pp. 2557–2560.

[24] S. Ghobrial, "Axial cross polarization in reflector antennas with surface imperfections," *IEEE Trans. Antennas Propag.*, vol. AP-28, no. 5, pp. 610–616, Sep. 1980.

[25] J. Jervase and S. Ghobrial, "Axial cross polarization in reflector antennas with surface errors of large correlation diameter," *IEEE Trans. Antennas Propag.*, vol. AP-31, no. 4, pp. 662–665, Jul. 1983.

[26] H. Ling, Y. Lo, and Y. Rahmat-Samii, "Reflector sidelobe degradation due to random surface errors," *IEEE Trans. Antennas Propag.*, vol. AP-34, no. 2, pp. 164–172, Feb. 1986.

[27] V. Chandrasekar and N. Bharadwaj, "Orthogonal channel coding for simultaneous co- and cross-polarization measurements," *J. Atmos. Ocean. Technol.*, vol. 26, no. 1, pp. 45–56, Jan. 2009.

[28] D. S. Zrnić, R. J. Doviak, V. M. Melnikov, and I. R. Ivić, "Signal design to suppress coupling in the polarimetric phased array radar," *J. Atmos. Ocean. Technol.*, vol. 31, no. 5, pp. 1063–1077, May 2014.

[29] M. C. Leifer, V. Chandrasekar, and E. Perl, "Dual polarized array approaches for MPAR air traffic and weather radar applications," in *Proc. IEEE Int. Symp. Phased Array Syst. Technol.*, Waltham, MA, USA, Oct. 2013, pp. 485–489.

[30] I. R. Ivic, "Quantification of polarimetric PAR effects on weather observables in the phase coded STSR mode," *IEEE Trans. Geosci. Remote Sens.*, vol. 60, 2022, Art. no. 5110022.

[31] A. Ryzhkov and D. S. Zrnic, *Radar Polarimetry for Weather Observations*. Cham, Switzerland: Springer, 2019.

[32] I. R. Ivic and R. J. Doviak, "Evaluation of phase coding to mitigate differential reflectivity bias in polarimetric PAR," *IEEE Trans. Geosci. Remote Sens.*, vol. 54, no. 1, pp. 431–451, Jan. 2016.

[33] I. R. Ivić, "Statistical evaluation of time multiplexing to mitigate differential reflectivity bias due to cross-polar coupling," *J. Atmos. Ocean. Technol.*, vol. 33, no. 1, pp. 127–147, Jan. 2016.

[34] Z. Li et al., "Polarimetric phased array weather radar data quality evaluation through combined analysis, simulation, and measurements," *IEEE Geosci. Remote Sens. Lett.*, vol. 18, no. 6, pp. 1029–1033, Jun. 2021.

[35] L. Borowska, "Analysis of weather data from the ten panel demonstrator (TPD) radar," NOAA/NSSL, Norman, OK, USA, Tech. Rep., 2020.